PROCEEDINGS OF SCIENCE

The first look at the coincidence of methanol and excited OH masers around HMYSOs

A. Kobak[a,*]

[a] *Institute of Astronomy, Faculty of Physics, Astronomy and Informatics, Nicolaus Copernicus University, Grudziadzka 5, 87-100 Torun, Poland*

E-mail: akobak@astro.umk.pl

Observational studies of high-mass young stellar objects (HMYSOs) at radio wavelengths are necessary to increase our understanding of high-mass star formation. Significant contributions to our knowledge of the formation of HMYSOs come from interferometric observations of cosmic masers, mainly OH, methanol, and water transitions. We imaged a sample of 12 sources where the excited OH maser line at 6.035 GHz exists and the 6.7 GHz methanol maser line using e-MERLIN. We present preliminary results for the first three targets, which are well-known high-mass star-forming regions. We find the spatial and spectral coincidence of maser clouds at both transitions and their avoidance. This allows us to put constraints on the local physical conditions in the close surroundings of HMYSOs.

15th European VLBI Network Mini-Symposium and Users' Meeting (EVN2022)
11-15 July 2022
University College Cork, Ireland

*Speaker

PoS(EVN2022)033

1. Introduction

Maser emission is an important tool for studying high-mass young stellar objects (HMYSOs). Using the maser lines it is possible to explore details of star formation processes [22] and physical conditions in the close surrounding of young stars [2, 3]. The 6.7 GHz methanol masers are the most common masers in HMYSOs. They occur in a wide range of kinematic temperatures and gas densities. The 6.035 GHz hydroxyl (OH) masers, so-called: excited OH masers (ex-OH), are also related to this early stage of star evolution. However, the existence of these transitions, coincidence or avoidance of each other, depends on the physical conditions of the gas surrounding the HMYSO. In Table 1 we summarize the required temperatures, densities, and dust temperatures as it is given by [2] for both maser transitions.

	Methanol 6.7 GHz	Ex-OH 6.035 GHz
Kinetic temperature	$T_k < 200$ K	$T_k < 70$ K
Gas density	$10^{5.5} < n_{H_2} < 10^{7.5}$ cm^{-3}	$10^{6} < n_{H_2} < 10^{8.5}$ cm^{-3}
Dust temperature	$T_d > 100$ K	$T_d > 20$ K

Table 1: Physical conditions required for methanol and excited OH maser emission based on [2].

During the star-formation processes, the magnetic field plays an important role in impacting the star formation rate, fragmentation process, and finally, the average mass of stars [10]. The magnetic field in the high-mass star-forming regions was widely examined in [18–20]. In these studies, the strength and direction of the magnetic field were examined, and a connection between the direction of the linear polarization vector and the outflow axis was analyzed. Here we present the first images obtained using the e-MERLIN interferometer of three HMYSOs: G69.540−0.976 (also known as ON1), G81.871+0.781 (also known as W75N), and G108.766− 0.986[1]. Their kinematic distances are 2.57±0.34 kpc [16], 1.30±0.07 kpc [17], and 2.81±0.23 kpc [15], respectively.

2. Observations

The observations were taken using e-MERLIN under the project CY10206 in full polarization (RR, RL, LR, LL) in 2020: 17 July (G69.540−0.976), 16 July (G108.766− 0.986), and 19 October (G81.871+0.781). Each source was observed in two frequency tunings, one covering the exited OH lines and the other the methanol line, interleaved closely in time to maximize the uv-coverage for either tuning. The observations were made at fixed frequencies corrected for the relative motion of the target with respect to the telescope on the observation date. They were correlated at Jodrell Bank Observatory. After pre-processing using the e-MERLIN CASA pipeline [13] data products included:

1) the wide-band data: four 128-MHz spectral windows (spws), each averaged to 128 channels per spw, 4 s integration time. These were observed at frequencies overlapping the relevant spectral lines.

[1]The names correspond to the Galactic coordinates.

2) the spectral line data (narrow-band): four 1 MHz spws, 512 channels per spw (separation 0.09 km s^{-1}), 4 s integration time. In one tuning, two spws were centered on the two main OH lines (6035.092 and 6030.747 MHz). In the other tuning, one spw was centered on the methanol line (6668.519 MHz). The total on-source time in each tuning was ∼1.4 hr (12 scans× 7 min).

The pipeline pre-processing included time- and frequency-dependent calibration of wide-band calibration sources including establishing a flux scale with respect to 3C 286 (J1331+3030), but no polarization calibration. Following the pre-processing we proceeded the standard steps for narrow-data reduction using CASA 5.8 (e.g. [5], [11]): (1) Remove any remaining bad data and calibrate the narrow-band data, including polarization. (2) Bandpass calibration: Apply the previous calibration: derive delay, phase, and amplitude corrections for the bandpass calibrator 3C 84 (J0319+4130), from the wide-band data to the narrow-band data, along with a correction for the phase offset between tunings. Perform time- and then frequency-dependent calibration to derive a bandpass correction table for amplitude and phase. Derive narrow-band bandpass table. (3) Assuming 3C 84 is unpolarised, apply the previous calibration to derive polarization leakage corrections. (4) Set the known polarization flux densities for 3C 286, apply the bandpass, leakage, and previous calibration, and derive the polarization angle correction. (5) Apply the previous calibration of the phase reference source to the target together with the corrections derived in steps (1-3) and the parallactic angle correction. (6) Split out the corrected target data, and transform the data to the LSR reference frame. (7) Select the brightest channel for self-calibration, taking care to maintain polarization accuracy. (8) Make spectral image cubes for each target in full polarization, setting the same restoring beam size of 45 mas×65 mas with position angle −50°, for both ex-OH and methanol transition. The following phase reference sources were used: J2010+3322 for G69.540−0.976, J2018+3851 for G81.871+0.781, and J2301+5706 for G108.776−0.986, respectively. The positions of maser spots were derived using the 2D Gauss fit – the JMFIT procedure in AIPS (NRAO 2022) [8].

3. Results and discussion

We successfully imaged the following three targets at both maser lines at the 6 GHz band: the 6.7 GHz methanol and 6.035 GHz ex-OH transitions. The remaining nine sources are in the process of calibration and imaging. Here, we analyze the maser spot spatial and spectral distributions and search for the Zeeman pairs at the ex-OH transition.

3.1 G69.540−0.976

The results for G69.540−0.976 are presented in Fig. 1. The 6.7 GHz methanol masers cover the region of 0.5"×1.1" (1220 au×2800 au for kinematic distance 2.57 kpc) with a trend of the red-shifted spots lying to the south and blue-shifted on the north. The emission appeared in the LSR velocity range from −0.5 km s^{-1} to 15.7 km s^{-1}. The radial velocity observed in the CH3CN line is 12 km s^{-1} [14]. The ex-OH masers at 6035 MHz appeared in a broader region of 1"×1.1" (2690 au×2770 au). Analyzing the maser spot spatial distributions at both transition and their LSR velocities, we report a partial coincidence of methanol and ex-OH masers. The coincidence of the

sky position is within a limit of 50 mas (130 au) and 0.9 km s^{-1} in the velocity domain. We also note, that two ex-OH maser groups in the central part of the masing region and one southern-east group appeared without any 6.7 GHz counterparts. According to the model of [2], that behavior can be an effect of a higher molecular hydrogen density and a low kinematic temperature, below 70 K, for the whole emission region. The region is associated with the young stellar object (YSO) IRAS 20081+3122, which is located south of the maser emission in the distance ~855 mas (~2200 au) from the point (0,0) ((ΔRA, ΔDEC)=(−100,−850) mas) [4]. The peak of radio continuum emission, which comes from the H$_{II}$ region is marked by a black star in Figure 1 [9]. The diameter of the H$_{II}$ region has 0.06 pc () and covers spatially the whole region of methanol maser emission.

We identified six Zeeman pairs at the 6035 MHz ex-OH maser line in this source. Considering the Zeeman splitting coefficient from [1], we calculated the strength of the line of sight magnetic field to be from −10 mG for the northern, blue-shifted features to −1.2 mG for the southern, red-shifted feature, where the minus sign indicates the magnetic field directed towards the observer.

3.2 G81.871+0.781

Figure 2 shows the results for G81.871+0.781. The methanol masers have a much more complex structure compared to ex-OH masers, but they appear in the same regions in the sky and the LSR velocity domain. The radial velocity observed in the CH_3CN line is 10 km s^{-1} [14] and in the HC_3N line is 10.9 km s^{-1} [12]. The methanol maser spots are spread over 0.5"×1" (640×1380 au for kinematic distance 1.3 kpc) and in the LSR velocity range from 2.6 km s^{-1} to 9.7 km s^{-1}, whereas the ex-OH emission over ca. 0.06"×0.3" mas (77×406 au) and from 6.2 km s^{-1} to9.2 km s^{-1}. All three groups of exited OH masers coincide with the methanol masers; the northern and southern groups coincide within 24 mas (31.2 au) and 0.5 km s^{-1}, and the middle group within 50 mas (65 au), and 0.4 km s^{-1} velocity domain. The brightest methanol emission occurs in the north, where no ex-OH emission is seen. We note, the methanol maser is weakening towards the south, where the ex-OH emission appears. That indicates a decline in the temperature and an increase in the density over the distance of 1" i.e. 1300 au. In the region are two peaks of millimeter continuum emission (MM1a, MM1b), that are traces of warm dust heated by the YSO [12]. The MM1b peak is marked in Figure 2. The second peak, MM1a, is in the distance ~1800 mas (~2340 au) from the (0,0) point on the southeast ((ΔRA, ΔDEC)=(886,−1610) mas), and is more compact and brighter than MM1b. Likely MM1a is responsible for H$_{II}$ region, which is southeast of masers emission in the distance ~1450 mas from (0,0) point ((ΔRA, ΔDEC)=(775,−1210) mas) [9]. A diameter of H$_{II}$ region is ~0.03 pc (~2400 mas), what means the masers appear on the edge of H$_{II}$ region.

We identified two Zeeman pairs that indicate the strength of the line of sight magnetic field of +7.3 and +8.5 mG in the middle ex-OH maser groups and +2.2 mG for the southern group. The field is directed away from the observer.

3.3 G108.776−0.986

The results for G108.776−0.986 are presented in Fig. 3. A clear separation between methanol and ex-OH maser emission is visible. Both masers appear on a compact area, smaller than the size of the beams; i.e. the 6.7 GHz methanol spots are spread over 8×10 mas (22×28 au for kinematic distance 2.81 kpc) and the 6.035 GHz ex-OH spots over 7×30 mas (20×85 au). The displacement

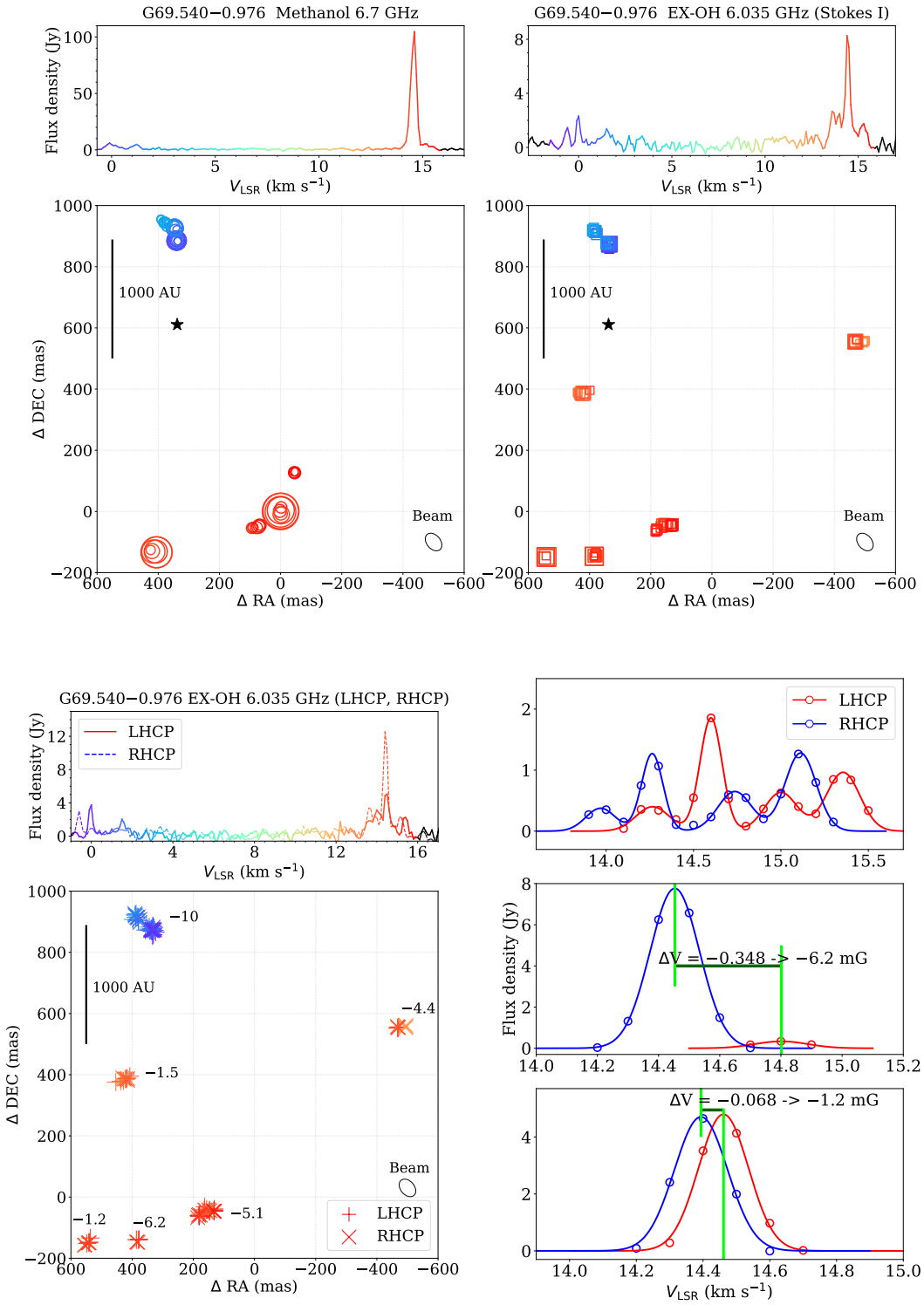

Figure 1: Top: The spectra and spatial distributions of the 6.7 GHz methanol (left) and 6.035 GHz ex-OH masers (right) in G69.540−0.976. The black star indicates the peak of the H_{II} emission. Bottom: The left- and right-polarizations (LHC, RHC) of ex-OH maser with the value of the magnetic field in mG (left) and the example of the Zeeman splitting measurements in three southern ex-OH masers (right).

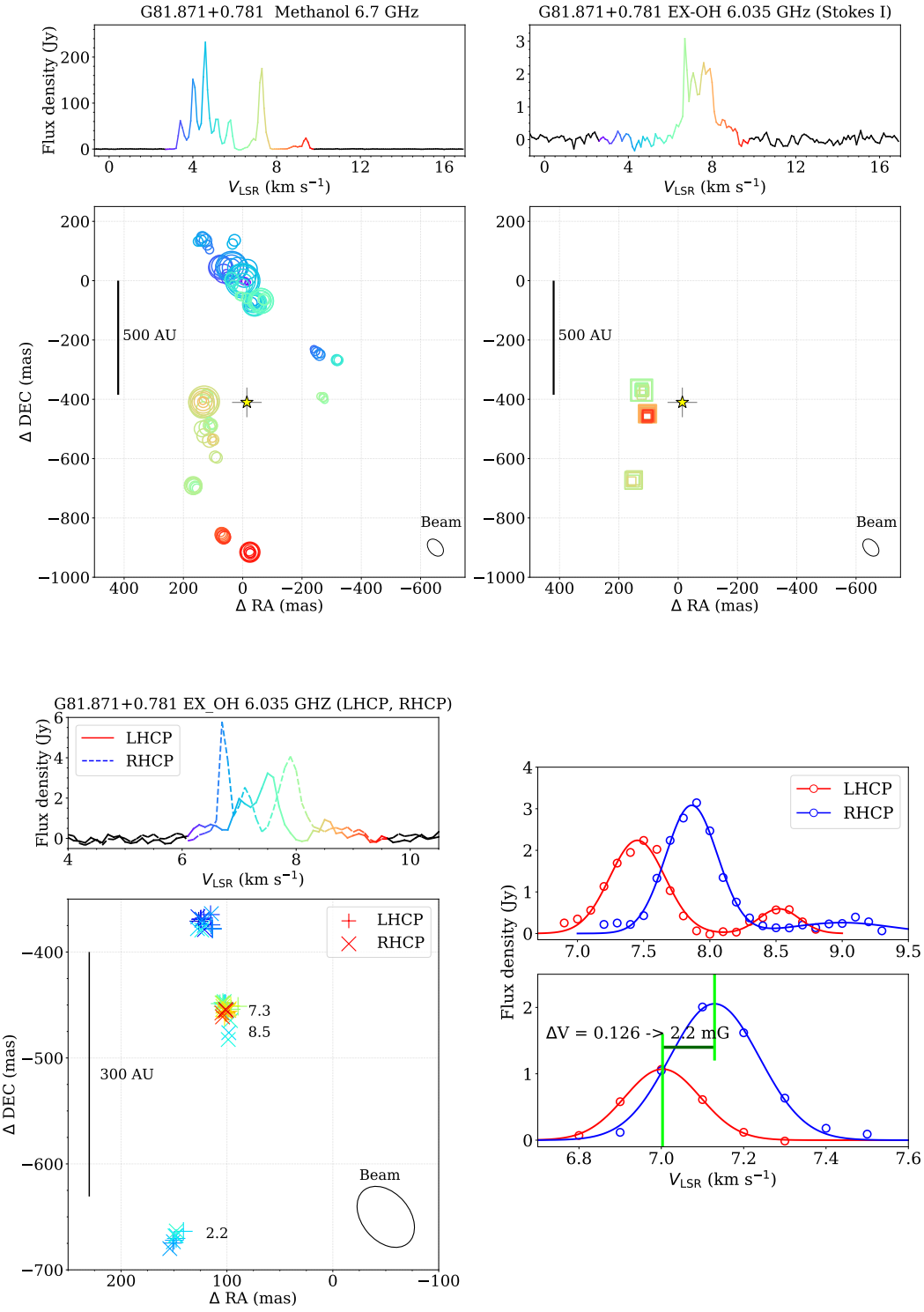

Figure 2: Top: The spectra and spatial distributions of 6.7 GHz methanol (left) and 6.035 GHz ex-OH masers (right) in G81.871+0.781. The yellow stars with grey cross indicate the position of the peak of MM1b core (1 mm continuum emission) with uncertainties. Bottom: The left- and right-polarized emission (LHC, RHC) of ex-OH masers with values of the magnetic field in mG (left) and the Zeeman splittings in two groups (right).

between the two maser lines is ∼50 mas (140 au) and indicates the existence of two regions, one hotter (with methanol masers) and the second denser and cooler (with ex-OH masers). The H_{II} emission was not noticed in G108.776−0.986 [9].

We identified two likely Zeeman pairs at the ex-OH transition. In both cases, the magnetic field was negative value, −8.5 and −10.6 mG, meaning that is directed towards the observer.

4. Summary

We successfully used e-MERLIN for the methanol and ex-OH maser imaging. Here, we present the first three targets from our larger sample of 12 HMSFRs. We showed that in two of them (G69.540−0.976 and G81.871+0.781), there is a likely coincidence of two maser transitions in the same gas volume. These regions are characterized by low kinetic (below 70 K) and high dust temperatures (over 100 K), and high gas density up 10^6 cm^{-3}. Moreover, in both targets, there are regions when either the 6.7 GHz masers or 6.035 GHz masers appear without any counterpart. This implies the differentiation of physical conditions at a scale of 1".

We estimate the magnetic field strength for each target based on the detected Zeeman pairs at the ex-OH maser transition. The results for G108.776−0.986 are −8.5 and −10.6 mG and are the first measurements presented in this region. In the case of G81.871+0.781, we obtained a similar value as [21] (within 0.3 mG) and as [18] (within 2 mG). In both cases, the magnetic field was measured based on the 6.7 GHz methanol maser. In G69.540−0.976 our obtained values of the red-shifted groups, −1.2 to −6.2 mG, are consistent with [7] and [6] within 1 mG, and the value of the blue-shifted group, −10 mG, agrees within 2 mG. The results [7] and [6] are based on ex-OH maser emission.

Acknowledgements

e-MERLIN is a National Facility operated by the University of Manchester at Jodrell Bank Observatory on behalf of STFC, part of UK Research and Innovation. We acknowledge support from the National Science Centre, Poland through grant 2021/43/B/ST9/02008.

References

[1] Baudry, A., Desmurs, J. F., Wilson, T. L., & Cohen, R. J. 1997, , 325, 255

[2] Cragg, D. M., Sobolev, A. M., & Godfrey, P. D. 2002, , 331, 521

[3] Cragg, D. M., Sobolev, A. M., & Godfrey, P. D. 2005, MNRAS, 360, 533

[4] Cutri, R. M. & et al. 2012, VizieR Online Data Catalog, II/311

[5] Darwish, M. S., Richards, A. M. S., Etoka, S., et al. 2020, , 499, 1441

[6] Fish, V. L. & Sjouwerman, L. O. 2010, , 716, 106

[7] Green, J. A., Richards, A. M. S., Vlemmings, W. H. T., Diamond, P., & Cohen, R. J. 2007, , 382, 770

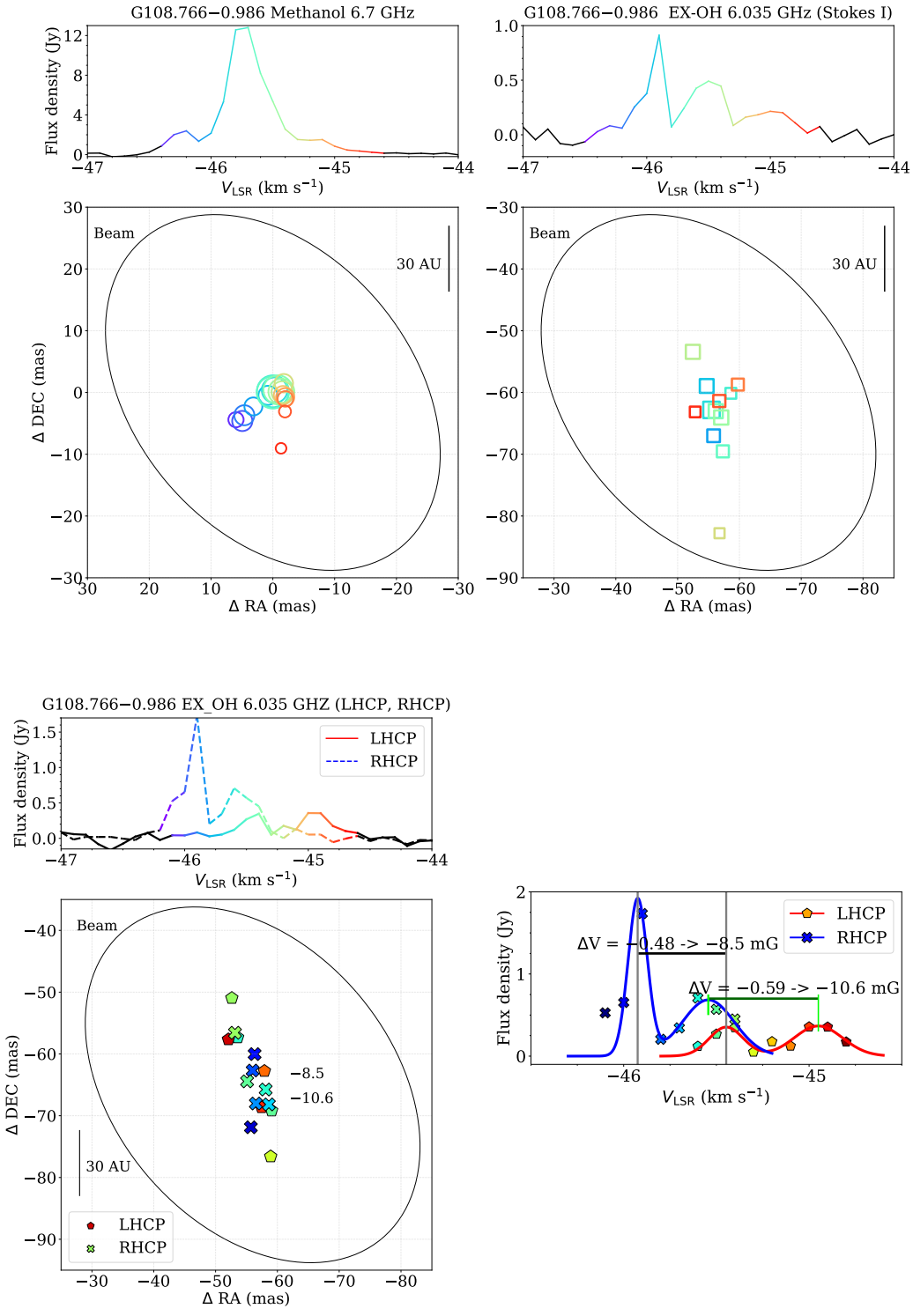

Figure 3: Top: The spectra and spatial distributions of 6.7 GHz methanol (left) and 6.035 GHz ex-OH masers (right) in G108.776−0.986. Bottom: The left- and right-polarized emission (LHC, RHC) of ex-OH masers with values of the magnetic field in mG (left) and the Zeeman splittings identified in this target (right).

[8] Greisen, E. W. 2003, in Astrophysics and Space Science Library, Vol. 285, Information Handling in Astronomy - Historical Vistas, ed. A. Heck, 109

[9] Hu, B., Menten, K. M., Wu, Y., et al. 2016, , 833, 18

[10] Krumholz, M. R. & Federrath, C. 2019, Frontiers in Astronomy and Space Sciences, 6, 7

[11] McMullin, J. P., Waters, B., Schiebel, D., Young, W., & Golap, K. 2007, in Astronomical Society of the Pacific Conference Series, Vol. 376, Astronomical Data Analysis Software and Systems XVI, ed. R. A. Shaw, F. Hill, & D. J. Bell, 127

[12] Minh, Y. C., Su, Y. N., Chen, H. R., et al. 2010, , 723, 1231

[13] Moldon, J. 2021, eMCP: e-MERLIN CASA pipeline, Astrophysics Source Code Library, record ascl:2109.006

[14] Pankonin, V., Churchwell, E., Watson, C., & Bieging, J. H. 2001, , 558, 194

[15] Reid, M. J., Menten, K. M., Brunthaler, A., et al. 2019, ApJ, 885, 131

[16] Rygl, K. L. J., Brunthaler, A., Reid, M. J., et al. 2010, , 511, A2

[17] Rygl, K. L. J., Brunthaler, A., Sanna, A., et al. 2012, , 539, A79

[18] Surcis, G., Vlemmings, W. H. T., Dodson, R., & van Langevelde, H. J. 2009, , 506, 757

[19] Surcis, G., Vlemmings, W. H. T., van Langevelde, H. J., Hutawarakorn Kramer, B., & Bartkiewicz, A. 2022, , 658, A78

[20] Surcis, G., Vlemmings, W. H. T., van Langevelde, H. J., et al. 2015, , 578, A102

[21] Vlemmings, W. H. T. 2008, , 484, 773

[22] Zinnecker, H. & Yorke, H. W. 2007, , 45, 481